https://doi.org/10.5194/egusphere-2025-5372
Preprint. Discussion started: 11 December 2025

Impact of South American biomass burning emissions on elevated South Atlantic upper tropospheric ozone

Linda Smoydzin[1], Vera Bense[1], Heiko Bozem[1], Philipp Joppe[1,2], Daniel Kunkel[1], Hans-Christoph Lachnitt[1], Holger Tost[1], Andreas Zahn[3], Helmut Ziereis[4], Martin Riese[5], and Peter Hoor[1]

[1]Institute for Atmospheric Physics, Johannes Gutenberg University, Mainz, Germany
[2]Aerosol Chemistry Department, Max Planck Institute for Chemistry, Mainz, Germany
[3]Karlsruhe Institute of Technology, Institute of Meteorology and Climate Research (IMK) Karlsruhe, Germany
[4]Institut für Physik der Atmosphäre, Deutsches Zentrum für Luft- und Raumfahrt (DLR), Oberpfaffenhofen, Germany
[5]Institute for Climate and Energy Systems (ICE-4), Forschungszentrum Jülich, Germany

Correspondence: Linda Smoydzin (smoydzin@uni-mainz.de)

Abstract. During the SOUTHTRAC mission in autumn 2019 elevated mixing ratios of carbon monoxide (CO), carbon dioxide CO_2, nitrogen oxide (NO) and total reactive nitrogen NO_y were observed during a flight at the beginning of October. The potential plume extended over more than 1000 km (15° latitude) east of the Brasilian coast at altitudes of 13 km in the upper troposphere. In-situ measurements showed elevated ozone in this plume (≈ 100 ppbv), being 20-40 ppbv higher than during a previous flight in early September at exactly the same flight route. For the plume flight positive correlations of ozone and pollutants (CO, NO, NO_y) indicate ozone production in these pollution layers. Lagrangian Analysis shows, that the observed air masses were strongly affected by biomass burning over Amazonia. A combined analysis of chemical Lagrangian box model and a global chemistry climate model (EMAC) revealed that ozone production from biomass burning predominantly caused the ozone enhancements. The effect is eventually intensified by NO_x produced from lightning. Upward transport of the plumes happened ≈ one week before the flight, allowing ozone to be formed and enhanced by 25% compared to the September flight. Estimates of the climate impact show, that the biomass burning produced ozone has a local effect on the radiative forcing of 50 mWm^{-2} .

1 Introduction

Ozone (O_3) is one of the most important anthropogenic greenhouse gases besides carbon dioxide (CO_2) and methane (CH_4) but has a larger uncertainty in its radiative forcing partly because of the highly variable source characteristics of ozone precursor gases such as nitrogen oxides (NO+NO_2=NO_x) and volatile organic compounds (VOCs). This holds in particular for wildfire emissions as well as the production strength of nitrogen oxides by lightning (LNO_x).

https://doi.org/10.5194/egusphere-2025-5372
Preprint. Discussion started: 11 December 2025

Biomass burning is an important source for tropospheric O_3 (Mauzerall et al., 1998; Duncan et al., 2007; Andreae, 2019; Schill et al., 2020) underlying however, strong regional and seasonal changes. Jaffe and Wigder (2012) estimate that approximately 3.5 % of global tropospheric O_3 formation is related to biomass burning emissions. Since the wildfire activity is projected to increase (Jacob and Winner, 2009; Torres et al., 2010; Yue et al., 2015; Abram et al., 2021), this source of O_3 will be more important in the future.

Trace gases emitted by fires can be transported into the upper troposphere and lower stratosphere (UTLS) and produce O_3 which acts as a greenhouse gas in these altitudes (Rap et al., 2015; Bozem et al., 2017; Xia et al., 2018; Bourgeois et al., 2021). Thus, perturbations of upper tropospheric (UT) ozone play an important role for the radiation budget of the atmosphere (Forster and Shine, 2002; Riese et al., 2012). Notably in the tropics and subtropics the impact of UT ozone on the local energy budget can be substantial (Rap et al., 2015).

To identify ozone production in observational data sets, positive correlations between O_3 and CO can be used. This is due to the fact that CO, NO_x and other ozone precursors are co-emitted by biomass burning as well as anthropogenic pollution sources. However, the correlation between O_3 concentrations and BB emissions is complex and highly non-linear leading mainly to ozone depletion in regions closer to the fire (e.g. Wentworth et al., 2018). Ozone production occurs mainly in larger distances downwind the fire, in particular in the mid- and upper troposphere (Real et al., 2007; Akagi et al., 2012; Parrington et al., 2013). The wide variation in net O_3 production within biomass burning smoke is related to several factors, including fire temperature, burning material and therefore differing emissions with respect to the emission strength as well as the ratios of the emitted species, all in combination with the prevailing meteorological conditions (e.g. Gilman et al., 2015; Koss et al., 2018; Andreae, 2019). Each of these factors influence the underlying RO_x (RO_x=OH, HO_2, and RO_2) chemistry that controls oxidation processes and secondary pollutant formation. Direct HO_x precursor emissions like formaldehyde (HCHO), acetaldehyde (CH_3CHO), and nitrous acid (HONO) show a great variability depending on the fire type and fire state (Liao et al., 2021; Kluge et al., 2020; Fiddler et al., 2024).

Tropospheric O_3 formation generally depends on the availability of NO+NO_2 (NO_x) and volatile organic compounds (VOCs) in the atmosphere (Leighton, 1961; Crutzen, 1974). It is common to divide O_3 formation regimes into NO_x sensitive (increase in NO_x leads to increase of O_3, changes in VOC's have little to no impact on O_3 mixing ratios) or VOC sensitive (further increase of NO_x leads to decrease of O_3) (Sillman, 1999). The resulting O_3 isopleths as a function of NO_x and VOC mixing ratios are often used to explain the different O_3 formation regimes (e.g. Seinfeld and Pandis, 2016). However, for a large range of scientific data analysis applications they are not applicable since (i) a large (box model) dataset is required to compose an O_3 isopleth diagram, (ii) knowledge of the mixing ratios of all atmospheric VOC compounds is hypothetically required, (iii) the method has been developed for (boundary layer) urban air pollution and is not necessarily applicable in the upper troposphere (Nussbaumer et al., 2023). Several approaches to use trace gas or production rate ratios as indicators for O_3 formation regimes have been developed in the past (e.g. Sillman, 1995; Tonnesen and Dennis, 2000; Tadic et al., 2020), but most of them are again not suitable for applications in the upper troposphere (Nussbaumer et al., 2023).

More than three decades ago, Fishman et al. (1990) and Watson et al. (1990) detected an O_3 maximum over the southern hemispheric Atlantic. Observational data from the SHADOZ network (Sauvage et al., 2006; Thompson et al., 2017; Witte

https://doi.org/10.5194/egusphere-2025-5372
Preprint. Discussion started: 11 December 2025

et al., 2017), satellite data (Edwards et al., 2003) and simulations with a global chemical transport model (Moxim and Levy II, 2000) indicate, that the region with elevated column O_3 level stretch over almost the entire tropical and northern sub-tropical South Atlantic. Convective uplift of biomass burning emissions (Chatfield and Delany, 1990; Pickering and Simpson, 1992; Kirchhoff and Marinho, 1994), the formation of nitrogen oxides by lightning (LNO_x) and long-range transport from South America and Africa to the Atlantic are supposed to contribute to the wave-one ozone maximum developing during September, October and November (SON) in the troposphere (Jenkins et al., 1997, 2021). The biomass burning season in South America is mainly concentrated between July and October, a period characterized by dry conditions associated with the decay phase of the South American monsoon system (Vera et al., 2006) while lightning activity reaches its maximum in SON over South America (Jenkins and Ryu, 2004). The number of convective events is largest in austral summer (DEC-FEB) however, they occur numerously and with a high variability with respect to the location and strength in all seasons. The relative contribution of biomass burning and LNO_x for the development of the South-Atlantic O_3 maximum is however, unclear (Edwards et al., 2003; Jenkins and Ryu, 2004; Sauvage et al., 2006; Jenkins et al., 2021). Using aircraft data over Brazil, trajectory data and ozone sonde data along the South-American east coast, Pickering et al. (1996) found evidence that uplift of biomass burning emissions in the vicinity of convective clouds in combination with lightning are the driving processes leading to the O_3 maximum over the SW-Atlantic. Pickering et al. (1996) estimate that the lightning contribution amounted to at least 32% of the measured NO_x mixing ratios.

For the tropical south Atlantic, Murray et al. (2013) estimate that LNO_x emissions are by far more important for O_3 production than biomass burning. Next to long range transport of biomass burning emissions and lightning NO_x production, downward transport of stratospheric air masses could contribute to the observed O_3 maximum. However, Liu et al. (2017) find that the contribution of biomass burning surface emissions exceed stratospheric impacts on O_3 formation over the northern South Atlantic.

Ulke et al. (2011) investigate transport patterns of biomass burning emissions from amazon forest fires. They conclude that in addition to convective uplift, the South American Low Level Jet (SLLJ) (Liebmann et al., 2004; Vera et al., 2006), a northerly wind east of the Andes mountains is all year round an important transport pathway of moisture and trace species from the Amazon to SE South America.

During austral summer, a band of high (convective) clouds develop regularly along the of South Atlantic Convergence Zone (SACZ) expanding from North-West Brazil (Amazon fire regions) to South-East Brazil. The SACZ can last quasi stationary for up to 8 days during austral summer, but it develops less intense also in austral spring (Liebmann et al., 2004; de Oliveira Vieira et al., 2013; Villela, 2017), representing another potential upper tropospheric outflow path for amazon BB emissions.

1.1 Motivation and objective

The SOUTHTRAC mission was carried out from September 2019 to November 2019 and consisted of two phases, with the HALO aircraft based in Rio Grande (Argentina) (Rapp et al., 2021). Inbetween the two phases HALO returned back to Germany, with the long transsects between South America and Germany carried out as measurement flights. This provided

https://doi.org/10.5194/egusphere-2025-5372
Preprint. Discussion started: 11 December 2025

several long flight legs in the UTLS across the Atlantic, on which we will focus on here.

During a flight at the beginning of October elevated upper tropospheric mixing ratios of CO, NO NO_y and O_3 were observed. The plume extended over more than 1000 km (15° latitude) east of the Brasilian coast. Measured O_3 mixing ratios in this plume (≈ 100 ppb), are about 20-40 ppbv higher than during a previous flight in early September at exactly the same location. The objective of our work is to locate the source region of the pollution layer and to quantify the contribution of biomass burning and lightning NO_x emissions to O_3 production by combining the observations obtained during the SOUTHTRAC mission and a set of model simulations.

2 Data and Methods

2.1 Instrumentation

HALO is capable of reaching flight altitudes of 14.5 km (49.000 feet) corresponding to pressure levels of 150 hpa. The aircraft was equipped with a comprehensive payload combining remote sensing and in-situ instruments. We focus here on in-situ measurements of carbon monoxide (CO), carbon dioxide (CO_2) nitrous oxide (N_2O) as well as ozone(O_3). CO, CO_2 and N_2O were measured with the UMAQS instrument (University Mainz Airborne Quantum Cascade Laser Spectrometer) from Johannes Gutenberg university Mainz (Müller et al., 2015; Kunkel et al., 2019). The instrument is in-situ calibrated against two secondary standards of different mixing ratios, which are compared to NOAA primary standards prior and after the campaign. Calibrations are carried out every 30-45 minutes to account for drifts of the instrument due to temperature driven changes of the optical path or the electronics. UMAQS is equipped with two astigmatic Herriot cells with an optical path lengths of 76 m (McManus et al., 2005). Cell pressure is stabilized at a cell pressure of 50 hPa. The time resolution is ultimately limited by the gas exchange rate in the cell as given by the pump speed and was at 1.5 s during SOUTHTRAC.

Estimated accuracy at flight level is 1.2 ppbv for N_2O and 2.5 ppbv for CO with a 1-sigma precision of 0.3 ppbv for N_2O and 2 ppbv for CO.

Ozone was measured with the Fast Airborne Ozone instrument (FAIRO), which combines UV photometry and chemoluminescence (Zahn et al., 2012). The time resolution is at 10 Hz, which is averaged to 1 s using a simple boxcar average giving an overall uncertainty of 2% for ozone.

Total reactive nitrogen (NO_y) and nitrogen oxide (NO) were measured by the AENEAS instrument ((Ziereis et al., 2022)).

2.2 Satellite data

2.2.1 MOPITT satellite data

To analyse upper tropospheric CO level over South America, we use thermal infrared level 3 data from the version 8 product of CO measurements derived from the MOPITT instrument (Deeter et al., 2019). Level 3 products are available as daily mean values on a 1x1° global grid. As MOPITT uses gas correlation spectroscopy of the thermal infrared radiation emitted from the

https://doi.org/10.5194/egusphere-2025-5372
Preprint. Discussion started: 11 December 2025

earths surface, it can retrieve vertical profiles for almost two independent layers of CO. Data products are available on 10 level with a vertical resolution of 100 hPa (surface, 900 hPa - 100 hPa).

2.2.2 GOES satellite data

To identify fire and lightning events, we use GOES-16 satellite data. GOES-16 is one of NOAA's geostationary satellites centered over 75°W, having a hemispheric coverage of 83° local zenith angle on the full disk mode providing observation measurements between 52° North and South. GOES-16 data cover the north- and south American continents and the adjacent oceans.

The Advanced Baseline Imager (ABI) is a 16-channel (2 visible, 4 nearinfrared, 10 infrared) passive imaging radiometer on board GOES-16. The Fire Detection and Characterization (FDC) product is one of the multiple GOES-16 ABI-derived baseline products (GOES-R Series Program , 2019, access date: 24.01.2025) It provides imagery of the Earth's surface and the atmosphere at very high spatial (2 km for infrared bands) and temporal (5 min) resolutions. Under clear-sky conditions, the minimum detectable size of a fire (mean temperature: 800 K) is estimated to be 0.004 km^2 at the sub-satellite point. It provides fire detection locations (latitude, longitude) and fire properties such as the fire radiative power.

The GOES-R Geostationary Lightning Mapper (GLM) instrument on board GOES-16 (GOES-R Algorithm Working Group and GOES-R Series Program, 2018, access date: 24.01.2025) is a single-channel, near-infrared optical transient detector that can detect the instantaneous changes in an optical scene, indicating the presence of lightning. GLM provides data of in-cloud, cloud-to-cloud and cloud-to-ground lightning activity with a spacial resolution of approximately 10km and a temporal resolution of 20 seconds.

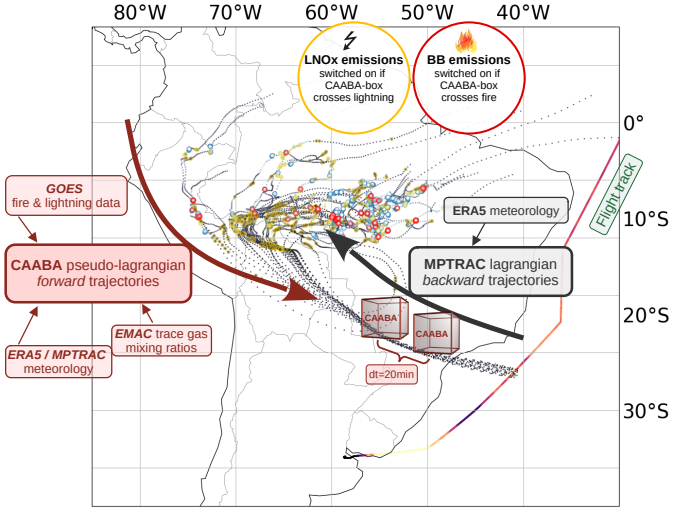

Figure 1. Schematic overview of the CAABA simulation setup.

https://doi.org/10.5194/egusphere-2025-5372
Preprint. Discussion started: 11 December 2025

2.3 Model description

To simulate the chemical and dynamical history of air masses being sampled along the HALO flight track, we use a combination of different model- and satellite data products:

2.3.1 Kinematic trajectory setup

To analyse the dynamical history of air masses, we calculate backward trajectories using MPTRAC (Hoffmann et al., 2016, 2022) which is a massive-parallel Lagrangian particle dispersion model allowing a computationally efficient calculation of transport simulations in the troposphere and stratosphere. A cluster of 240 trajectories is started every 5 minutes in a square of 0.25° surrounding the flight track. The backward simulation time of each trajectory is 13 days. MPTRAC simulations are driven with meteorological data from the ECMWF (European Center for Medium-Range Weather Forecast) ERA5 atmospheric reanalysis data set (Hersbach et al., 2020).

2.3.2 Chemical Lagrangian analysis

To analyse the chemical processing of air masses before they reach the flight path, we use the chemical box model CAABA (Sander et al., 2019) in a pseudo-lagrangian way to calculate atmospheric chemistry along each trajectory calculated with MPTRAC (fig. 1). Chemistry simulations using the CAABA box model are initiated at the last MPTRAC timestep and are calculated every 20 minutes in the forward mode along each trajectory until the flight path is reached (see fig2). The procedure is similar as in Riede et al. (2009) but with numerous extensions in CAABA: (i) Meteorological conditions (temperature, pressure, humidity, geographical position of the air mass) used in CAABA are taken from the trajectories calculated with MPTRAC (i.e. ERA5 meteorology). (ii) Gas phase chemistry is calculated using MECCA/MIM (Pöschl et al., 2000; Sander et al., 2019) which is the same chemical mechanism as used by EMAC and as applied by Nussbaumer et al. (2023).(iii) Chemical trace species are initialised with mixing ratios obtained from a simulation with the EMAC model (Jöckel et al., 2016) with a resolution of T42L90MA similar as in Jöckel et al. (2016). (iv) We implemented an algorithm, to account for turbulent mixing of air masses in the CAABA-box with background air masses outside the chemical box model. For ambient trace gas mixing ratios we use again data from the EMAC simulation. The mixing strength is scaled with the Richardson number which is calculated based on ERA5 data. (v) Aerosol phase chemistry is not calculated explicitly but heterogeneous reactions on aerosol particles are parameterised using a climatological aerosol size distribution obtained again from EMAC data. (vi) To calculate photolysis rates in CAABA/MECCA, ERA5 cloud data and O_3 column data from EMAC are used. (vii) Anthropogenic emissions from the IPCC RCP6.0 emission inventory are used (Pozzer et al., 2009; van Vuuren et al., 2011). All required quantities (satellite data products, 3d-model data) are sampled and interpolated to the trajectory position in space and time.

The calculation of biomass burning emissions follows the procedure of Kaiser et al. (2012). However, we use instantaneous fire radiative power data from the GOES satellite instead of the assimilated GFAS product (eqn. 35, 36 in Kaiser et al., 2012).

https://doi.org/10.5194/egusphere-2025-5372
Preprint. Discussion started: 11 December 2025

The dry matter combustion rate $f(DM)$ for each located fire is calculated as

$$f(DM) = \sum_{i=1}^{8} \delta_{i,l} \beta_i \rho \quad (1)$$

where ρ is the fire radiative power, l,i $\in$ [1,8] denotes the land cover class at the fire location which is taken from table 2 in Kaiser et al. (2012) like the conversion factor β. The emission rate density $f(s)$ for smoke constituents s is defined as:

$$f(s) = \kappa(s) f(DM) \quad (2)$$

The species emission factors are taken from Andreae and Merlet (2001) with updates from Akagi et al. (2011). The technical implementation of biomass burning emissions into CAABA follows Cabrera-Perez et al. (2016). Biomass burning emissions in CAABA are switched on, if air masses cross a fire detected by GOES and air masses are within the (ERA5) boundary layer (BL).

Subsequently lightning NO_x emissions are switched on in CAABA, if the trajectory crosses a lightning event detected by the GLM sensor on board GOES-16. The estimate of the lightning NO_x (LNO_x) emissions has generally a high uncertainty. Schumann and Huntrieser (2007) give an average lightning induced production of 250 mol NO per flash. In a 3d model this emission is added partially over several model level along a C-shaped profile (e.g. Pickering et al., 1998). We chose a LNO_x emission factor leading to the addition of approximately 0.02 ppb NO per CAABA timestep. This value is chosen following Cuchiara et al. (2020) who investigate chemistry in the outflow of a convective plume using a parcel model.

2.3.3 O_3 production metric

Due to the deficiencies of current metrics to classify ozone production regimes in the UT, Nussbaumer et al. (2022) have developed a novel method to investigate O_3 formation regimes which is still valid outside the atmospheric boundary layer. Their method is based on the idea, that O_3 formation in the upper troposphere can be described by the reaction between NO or HO_2 and peroxy radicals, the latter being approximated by CH_3O_2 accounting for $\approx$85% of all peroxy radicals in the upper troposphere (Nussbaumer et al., 2021, 2023). While the production of HCHO via reaction of CH_3O_2 with NO or OH enhances O_3 formation, the reaction between CH_3O_2 and HO_2 leads to the formation of CH_3OOH terminating the HO_x cycle and leading to a deceleration of O_3 formation. This relationship is defined by Nussbaumer et al. (2023) with the term $\alpha_{(CH_3O_2)}$

$$\alpha_{(CH_3O_2)} = \frac{k_{(CH_3O_2+NO)} * [NO] + k_{(CH_3O_2+OH)} * [OH]}{k_{(CH_3O_2+NO)} * [NO] + k_{(CH_3O_2+OH)} * [OH] + k_{(CH_3O_2+HO_2)} * [HO_2]} \quad (3)$$

where k is the rate coefficient for the reactions given in the brackets. Note, that the reaction between CH_3O_2 and OH is not included in the MIM chemical reaction mechanism due to its slow turnover time.

2.3.4 CAABA simulation scenarios

To analyse MPTRAC/CAABA trajectories, we assort them into different categories. Trajectories (i) which cross fires while they are in the BL (BB, all of these trajectories also cross lightning regions), (ii) which cross lightning regions with previous

https://doi.org/10.5194/egusphere-2025-5372
Preprint. Discussion started: 11 December 2025

continental BL contact ($FLASH\_BL$), (iii) which cross lightning regions without continental BL contact ($FLASH\_noBL$),
200 (iv) which neither cross fires nor lightning regions ($REST$).

BB	biomass burning + LNOx + anthropogenic emissions
$FLASH\_BL$	LNOx + anthropogenic emissions
$FLASH\_noBL$	LNOx emissions
$REST$	

Table 1. CAABA simulation scenarios.

3 Results

3.1 Observations

We will focus on the southern hemispheric parts of two transects of the SOUTHTRAC campaign between Europe and Rio
205 Grande, i.e. flight ST06 on 08.September 2019 and flight ST19 on 07.October 2019 (Fig.3). Both flights provided UTLS data at ≈ 13.5 km altitude and potential temperature levels of Θ between ≈ 348 and 360 K (fig 3). The composition of the subtropical UT in the latitude range between ≈ 30° and 10°S changed substantially between ST06 and ST19, as indicated by Fig. 2. During 7. October, the named region shows strong enhancements of CO, CO_2, NO, NO_y as well as O_3 mixing ratios compared to 8. September. Notably the enhancements are well positively correlated during the October flight, which hints
210 towards partly common sources and ozone production.

Overall the data indicate, that strong pollution was encountered over this part of the flight as also pointed out by Johansson et al. (2022). They concluded on the basis of GLORIA observations, that biomass burning contributed to a large extent to the observed tracer perturbations during flight ST19.

215 3.2 Synoptic conditions and trajectories

Potential vorticity level from ERA5 indicate that both flights in the considered latitude range took place in the upper subtropical troposphere at PV levels between PV=0 and PV=-3.0 pvu.

During the seven days prior the flights, synoptic conditions over South America were significantly different. The South Atlantic subtropical high (SASH) was positioned relatively stable over the south-west Atlantic between 40°-20°W and 40°S during the
220 beginning of October 2019 (ST19) while at the beginning of September (ST06) a strong low pressure system passed southern South America and impacted the atmosphere up to latitudes north of 30°S (supplement fig. S4). Therefore, the tropospheric outflow pattern is much more homogeneous in October compared to September. This is supported by a series of forward trajectories starting in six hourly time intervals at the surface over the Amazon Basin (in a square between 80°W , 50°W and 5°S, 15°S) on 01 September indicating very heterogenous transport pathways to the Atlantic over a broad altitude range.

https://doi.org/10.5194/egusphere-2025-5372
Preprint. Discussion started: 11 December 2025

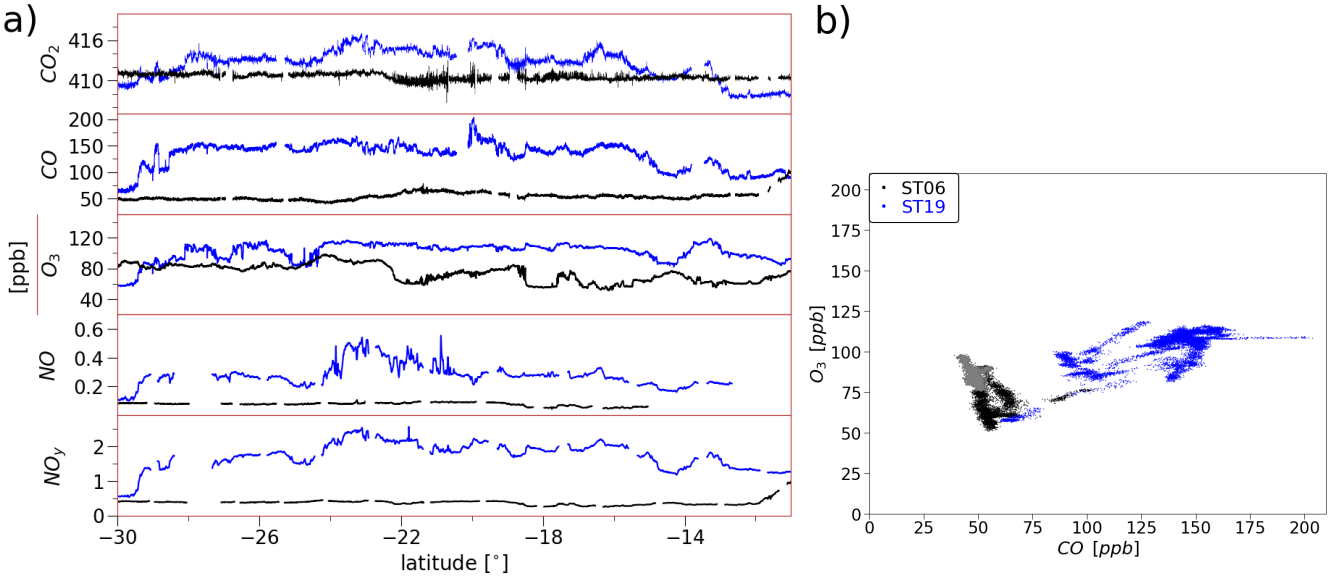

Figure 2. Latitudinal cross section for various chemical tracers measured during the transfer flights (a) from and to Buenos Aires (on 08.09.2019 (black) and four weeks later (07.10.2019, blue). The correlation between observed O_3 and CO mixing ratios are shown in b). Grey dots mark mixing ratios of flight ST06 south of -22.75.

GOES satellite data show a continuous band of high reaching clouds stretching from North-West Brazil to South-East Brasil the first days of October indicating, in combination with ERA5 surface charts, a well defined SACZ.

Figure 3 shows all simulated backward trajectories being initiated south of 5°S. A large number of ST19 trajectories descend into the atmospheric boundary layer crossing fires over South America (Fig.3a) while this fraction is negligibly small for ST06 (Fig. 3d). The same holds generally for the number of boundary layer contacts over the South American continent which are less for ST06 compared to ST19 (fig.3 a,b,d,e). Numerous trajectories cross lightning regions while being in the upper troposphere for both flights, however, the number of trajectories as well as the number of crossed lightning events is much larger for ST19 than for ST06 (fig. 3 a,b,d,e). It is also obvious, that flow patterns differ for both flights. BB and $FLASH$ trajectories for ST19 circle over South America while they show predominantly a westerly flow for ST06.

On average, backward trajectories need ≈ seven days to have boundary layer contact for both flights. In general, boundary layer (BB) trajectories are lifted rapidly into the upper troposphere after fires have been crossed even though they do not explicitly experience convection in a lagrangian transport model. Since solely the grid scale vertical velocity is considered to calculate vertical motion in MPTRAC, it is likely, that we rather underestimate than overestimate the number of uplifted BB trajectories. Generally, convective activity over South America is high in September and October as well as fire activity. The number of fire counts detected by the GOES fire detector does not differ significantly between ST19 and ST06. Neither does the average fire radiative power or the fire regions.

https://doi.org/10.5194/egusphere-2025-5372
Preprint. Discussion started: 11 December 2025

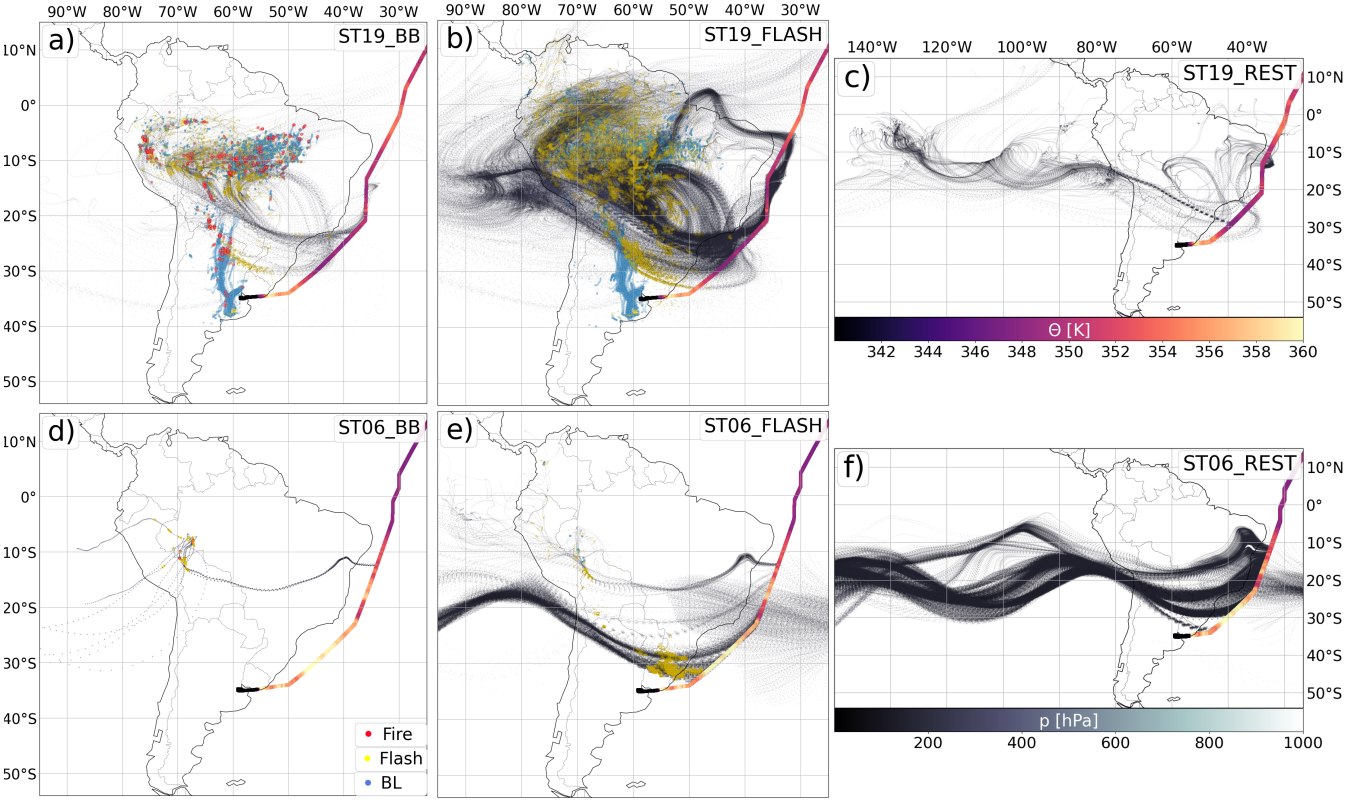

Figure 3. Plots show the pressure [hPa] (see colour code (f)) along all backward trajectories being started south of 10°S for flight ST19 (a,b,c) and ST06 (d,e,f) for each simulation scenario defined in section 2.3.4, table 1: BB (a,d), FLASH (BL+noBL) (b,e), REST (c,f). Red circles mark the time of biomass burning emissions, yellow circles the time of LNO_x emissions and blue circles the time of boundary layer contact. Θ along the flight track is shown in all plots (see colour code (c))

3.3 Chemistry

We focus our trace gas analysis on the latitude range between -30° and -11°S where HALO flew at a constant pressure level of 179 hpa (pv between 0 and -1 PVU) during ST19 related to O_3 mixing ratios of almost constantly 115 ppbv and CO mixing ratios of 150 ppbv. During ST06 the flight level increased from 161 hPa north of -22°S to 146 hPa further south. This ascent of the airplane is associated with an increase of O_3 mixing ratios to 80-100 ppbv which are south of -22° approximately the same order of magnitude as during ST19. The increase of O_3 is however related to a decrease in CO mixing ratios, a decrease towards stratospheric values of ERA5 pv level along the flight track from 0/-1 to -2/-3 and a descending vertical wind in the ERA5 data south of -22°. Therefore it is unlikely, that trace gas mixing ratios in this region are impacted by polluted boundary layer air masses. Absolute mixing ratios of CO are continuously smaller than O_3 mixing ratios in the considered latitude range for ST06 (vice versa for ST19) indicating unpolluted air in the upper troposphere and eventually stratospheric influence. The latter is however weak as O_3 mixing ratios increase between -22° and -30° but they are still below 100 ppbv and N_2O mixing

https://doi.org/10.5194/egusphere-2025-5372
Preprint. Discussion started: 11 December 2025

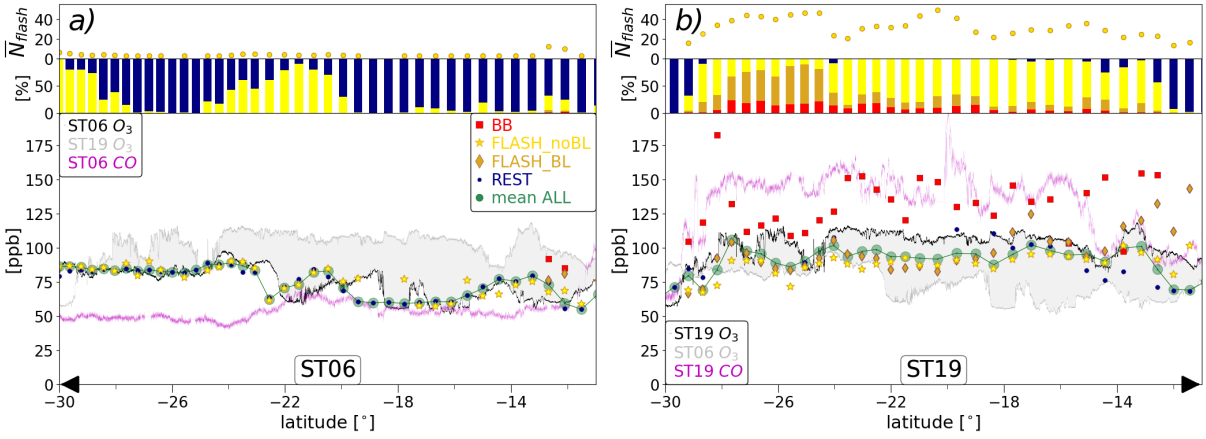

Figure 4. Plots show observed O_3 (black + grey line) and CO (purple line) mixing ratios along the flight track of ST06 (a) and ST19 (b). The grey shaded area indicates the differences in observed O_3 mixing ratios between flights ST06 and ST19. Coloured marks give the simulated trajectory mean of each simulation scenario ($BB, FLASH\_BL, FLASH\_noBL, REST$, see legend in a)) and the mean of the entire trajectory ensembles ($meanALL$) consisting of 200 trajectories starting every 5 minutes along the flight track.
The bars give the fraction of trajectories belonging to each simulation scenario and yellow dots in the top row give the average number of lightning events for each trajectory ensemble.

ratios are in the tropospheric range. Clearly, air masses during both flights (ST06, ST19) represent significantly different atmospheric regimes (fig.2b).

To investigate the reason for the strong ozone enhancements in more detail and the chemical history of the air masses during ST19, we have applied the CAABA box model along all trajectories shown in Fig. 3.

We compare the observations with the means of the entire trajectory ensembles (consisting of 240 trajectories, green circles) and the mean of of each simulation scenario (table1) having the same start time (i.e. 5 min time interval) at the flight track position.

Comparing the different simulation scenarios, it is evident that O_3 mixing ratios of scenario $ST19\_BB$ (red squares, Fig.4b)) are much higher than for all other simulation scenarios and are much higher than the observations (black line). However, the simulated O_3 of the entire trajectory ensemble means (green circles, Fig.4b) generally agree well with the measurements along the flight track, though the model slightly underestimates O_3 mixing ratios (green circles vs. black line, 4b). Lightning affected O_3 mixing ratios along all FLASH trajectories (yellow stars, brown diamonds) are almost always below observational values for ST19 with an exception north of -18°. Here the analysis showed that $FLASH\_BL$ trajectories receive a significant amount of anthropogenic (VOC) emissions followed by enhanced O_3 formation.

Figure 5 shows the net O_3 production in relation to NO mixing ratios and $\alpha_{(CH_3O_2)}$ at the time of: (a) biomass burning emissions and (d,e,f) LNOx emissions. Production of O_3 (P(O_3)) is clearly highest for BB trajectories at the time of BB emissions when both NO and VOC mixing ratios are high ($\alpha_{(CH_3O_2)}$ small). Furthermore, enhanced P(O_3) is indicated at the time of LNOx emissions when air masses are in the upper troposphere but still carry sufficient amounts of biomass burning trace gases

https://doi.org/10.5194/egusphere-2025-5372
Preprint. Discussion started: 11 December 2025

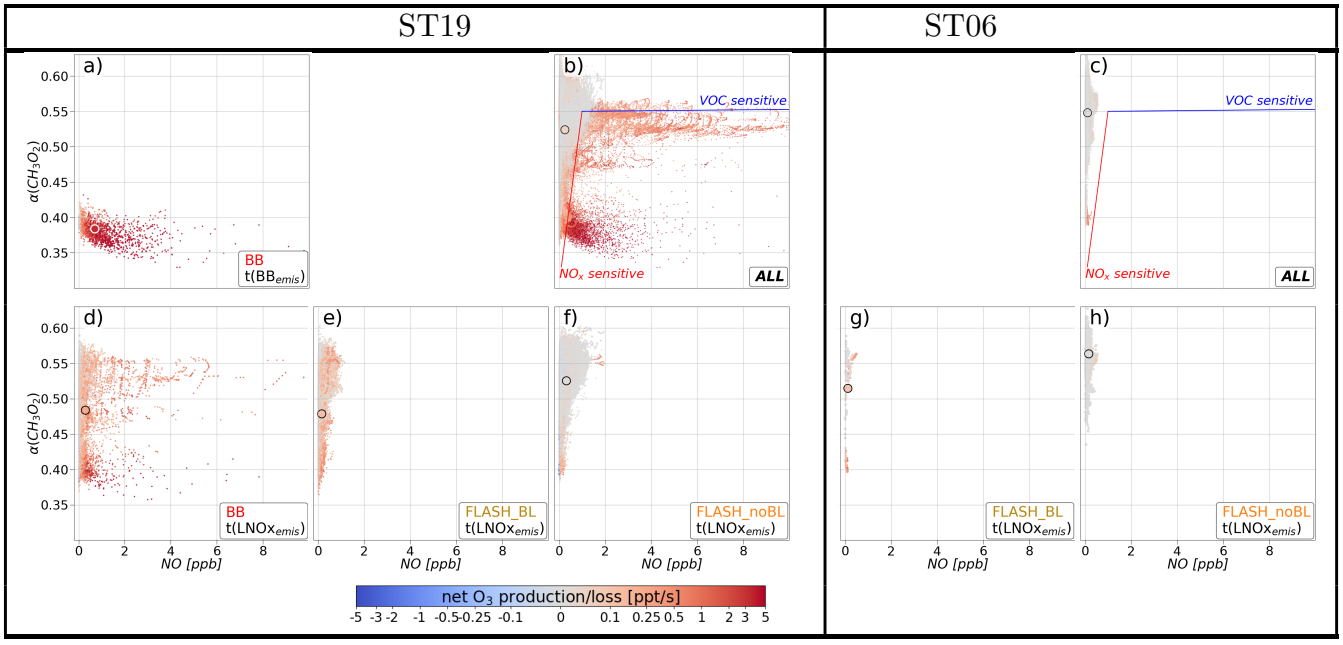

Figure 5. Simulated daytime O_3 as a function of NO mixing ratios and $\alpha_{(CH_3O_2)}$ at all trajectory positions (b,c), at the time of biomass burning emissions $t(BB_{emis})$ (a) and at the time of lightning emissions $t(LNOx_{emis})$ (d-h). All Plots except b) and c) show a selection of trajectories: (a,d) biomass burning (BB) trajectories, (e,g) lightning trajectories which had BL contact (FLASH_BL) and (f,h) lightning trajectories without BL contact (FLASH_noBL). The large circle marks the mean of all trajectory points.

(5 d). Production rates of O_3 are also much higher for $FLASH\_BL$ (fig.5e) compared to $FLASH\_noBL$ trajectories (fig.5f), which highlights the importance of boundary layer emissions for the chemical processing in uplifted air masses.

Simulated NO mixing ratios are on the same order of magnitude as observations, with a slight northward shift of the observed pattern, i.e. the observed maximum (supplement fig. S3 and fig. 2a)). The amount of emitted NO per flash underlays a large uncertainty. Enhancing LNOx emissions leads however, only to a significant overestimation of NO mixing ratios while P(O_3) does not increase significantly as air masses in the regions of lightning are mainly in a VOC sensitive regime, (fig. 5 f)) in particular for all $FLASH\_noBL$ trajectories (fig. 5 f),h)).

It is likely that the amount of (biomass burning) surface emissions, especially local emission maxima are underestimated in the CAABA simulations as we use initial and boundary conditions from EMAC on a 1°x1° grid. This also means, that the impact of fire emissions nearby any given trajectory position on the composition of air masses at the trajectory position itself might be tremendously underestimated. Additionally, we might miss fires when they are close to but not exactly at the trajectory position. Furthermore, the time of LNOx emissions in CAABA is based on satellite data which are independent of ERA5 data driving the MPTRAC trajectories. Therefore, convective activity in ERA5 is rather small at some locations where GOES detects lightning events which are most likely connected to an uplift of boundary layer air masses into the UT. In addition, it is possible, that we generally underestimate the number of BL trajectories as mentioned in 3.2.

https://doi.org/10.5194/egusphere-2025-5372
Preprint. Discussion started: 11 December 2025

Therefore, we performed a second set of CAABA simulations for ST19, adding additional VOC emissions in CAABA for cases, when CAPE in ERA5 is greater than 1000 J kg^{-1} and flashes were observed but trajectories had no BL contact before (scenario $FLASH\_noBL$). In these sensitivity simulations O_3 formation of numerous FLASH trajectories is larger also leading to higher trajectory mean O_3 mixing ratios (in particular between -24° and -18°S, supplement, fig. S1) agreeing very well with the observations.

For ST06, simulated O_3 mixing ratios (green circles vs black line) agree very well with the observations. CAABA simulations only show a southward shift of the local O_3 maximum at ≈ -19°S. The fact that the number of BL contacts for ST06 trajectories is negligibly small (or zero), related to small upper tropospheric mixing ratios of VOCs and NO_x explains the much smaller O_3 mixing ratios during ST06 (especially north of -22°) compared to ST19. In the latitude range between -24° and -20°S, the majority of trajectories cross lightning regions (detected by GOES) however, the number of flashes per trajectory is on average much small than for ST19 trajectories. Again, CAABA air masses are in a VOC sensitive regime at the time of LNOx emissions (fig.5g,h) thus adding LNOx would not lead to higher P(O_3) production. However, in contrast to ST19, simulated mean O_3 mixing ratios for ST06 agree well with observations without the injection of additional VOCs.

Lightning events in ST06 (between -24° and -20°) are close to the flight track over coastal regions. It is likely that air masses which are lifted convectively there (in the vicinity of lightning) carry rather clean (marine) air into the UT rather than polluted air explaining the good agreement even though MPTRAC trajectories have no BL contacts at all.

Generally, simulated O_3, VOC and NO_x mixing ratios for $FLASH\_noBL$ scenarios are higher (4, 5f,h) for ST19 compared to ST06 even though for both flights these trajectories remain in the upper troposphere at similar pressure levels throughout the backward simulation time. All trajectories are initiated and nudged with EMAC data representing the background atmosphere which is also severely impacted by biomass burning in October compared to the beginning of September.

Therefore, we can finally conclude that solely in the presence of sufficient VOC and NO_x mixing ratios, the observed amount of O_3 can be produced and that required VOC mixing ratios are of orders of magnitude needing a very strong emission source such as biomass burning. ST19 trajectories have almost solely BL contact in rain forest regions, where anthropogenic emissions are small. In addition, observed CO mixing ratios of ≈ 150 ppb give very strong indications, that biomass burning emissions contribute predominantly to the pollution layer over the subtropical Southern Atlantic during ST19.

3.4 Satellite data

To address the question of the representativeness of the SOUTHTRAC observations, we compare observed CO mixing ratios with long term MOPITT satellite observations. As mentioned above, we observe up to 100 ppbv higher upper tropospheric CO mixing ratios during ST19 compared to ST06. The same difference can be seen in the EMAC mixing ratios and therefore in the CAABA simulations as well as in MOPITT CO data. Comparing the 10 day mean of MOPITT CO mixing ratios prior the flight days (the trajectory backward simulation time), CO is significantly higher at 400 hPa, 300 hPa as well as 200 hPa for ST19 compared to ST06 (Fig.6b). This is generally not surprising since flight ST06 took place in the beginning of the South American biomass burning season and flight ST19 in the mid/end of the burning season.

https://doi.org/10.5194/egusphere-2025-5372
Preprint. Discussion started: 11 December 2025

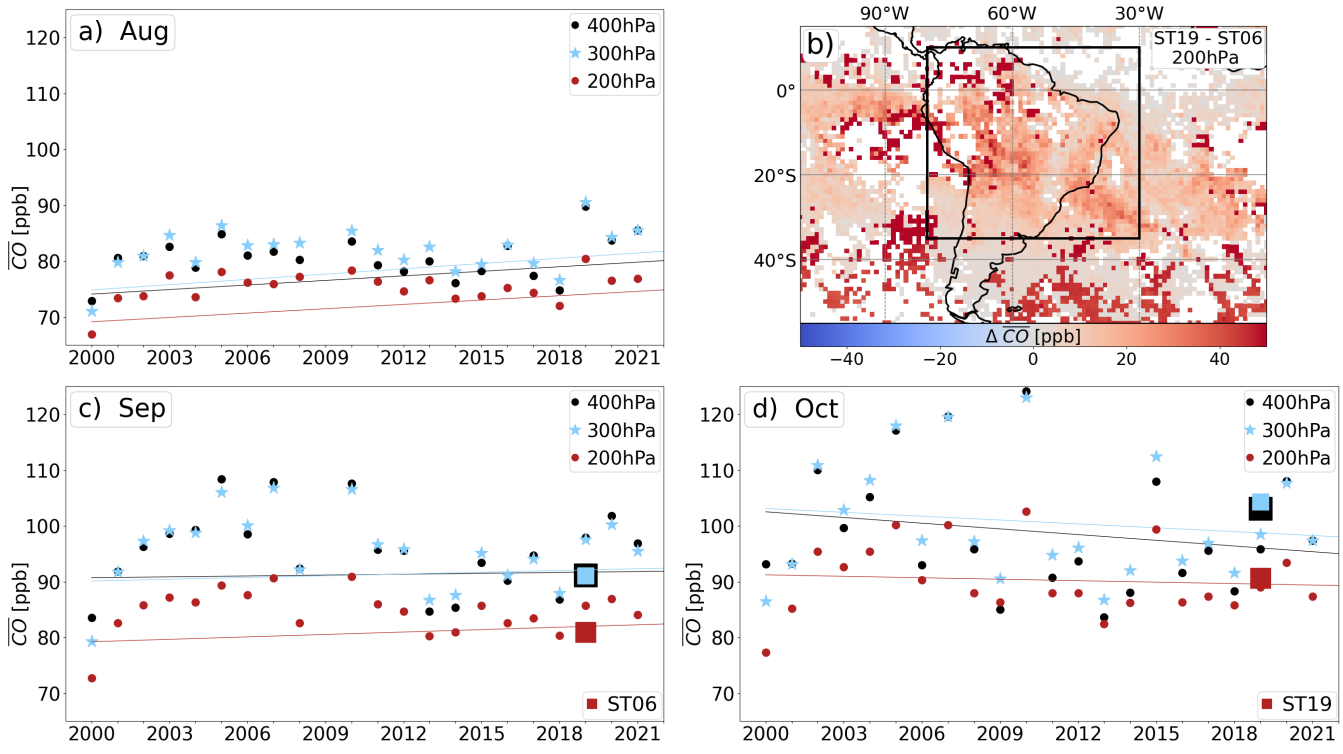

Figure 6. Plot b) shows differences in CO mixing ratios derived from the MOPITT satellite instrument for the 10 days prior flight ST06 (29.08-08.09 2019) and ST19 (28.09.-07.10.2019). Plots a),c), d) show a climatology of CO monthly mean mixing ratios from MOPITT over South America (square in b)) at 400 hPa (black), 300 hPa (yellow) and 200 hPa (red). Squares show the 10 day CO mean prior flights ST06 (c) and ST19 (d).

Figure 6 (a,c,d) shows the 23 years climatology of mean MOPITT CO mixing ratios over South America (mean for region in black square in Fig. 6b) for August, September and October at 400 hPa, 300 hPa and 200 hPa. Clearly visible are higher CO mixing ratios throughout the upper troposphere in October compared to August. The 10-day CO mean values for flight ST06 are close to the regression line of the climatology for September for all three shown pressure level.

For ST19, the 10 day mean at 200 hPa agrees also well with the climatological mean while values at 300 and 400 hPa are slightly above the mean (also the 2019 October mean). However, CO mixing ratios at these pressure levels have a much larger inter-annual variability in October compared to August and September. Therefore, we can conclude that conditions before/during both flights are not exceptional but rather typical of the time of year (i.e. beginning of September and October) and region.

https://doi.org/10.5194/egusphere-2025-5372
Preprint. Discussion started: 11 December 2025

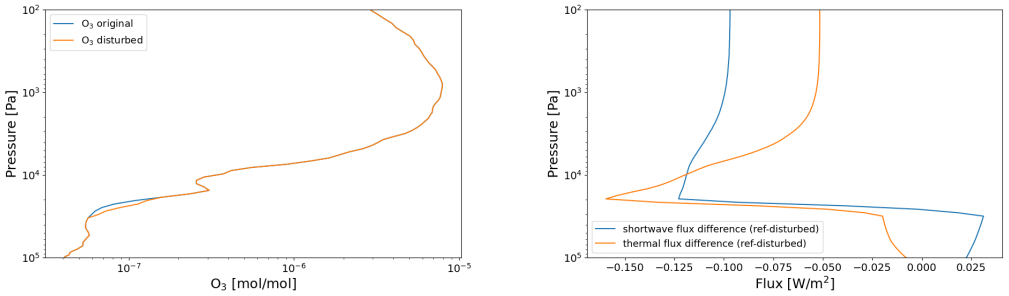

Figure 7. Estimated effect of the ozone perturbation (left) as observed during ST06 and ST19 on the radiative fluxes in the UTLS (right) showing a reduction of the radiative fluxes of 0.1 Wm^{-2}.

3.5 Consequences for the radiation budget

To estimate the effect of the perturbed ozone on the radiation budget, we applied a modification of the ozone profile in the UTLS as observed during the flights to the simulated background ozone field. We used a 1D-column model with the same radiative code as in the global EMAC model as described above. As shown in Fig.7 we find a reduction of both, shortwave and longwave fluxes in the stratosphere which peaks in the UTLS. It reduces radiation from the troposphere and therefore reduces absorption in the stratosphere. The enhanced ozone at the cold tropopause further reduces LW-fluxes towards the surface. The shortwave fluxes are reduced as well. Notably, this only reflects the impact of ozone without accounting for aerosols or water vapour co-emitted by the fires. The numbers are in line with estimates of the radiative kernel by Rap et al. (2015) who found sensitivities of approximately 3-5 mW m^{-2}/ppbv/100 hPa, which would correspond to 90-150 mW m^{-2} net forcing for an ozone perturbation of 30 ppbv in a layer of 100 hPa (compare Fig.2).

4 Discussion and Conclusions

The two transect flights of the SOUTHTRAC mission provide a unique dataset of the upper tropospheric composition. To our knowledge, the observation of a southern hemispheric upper tropospheric O_3 maximum extending several hundred kilometers from -11° -30° has not been reported before, in particular not at a pressure range between 146 and 179 hPa.

Based on our analysis combining box model simulations, EMAC model data as well as MOPITT satellite data, we can conclude that biomass burning emissions contribute predominantly to the enhanced upper tropospheric O_3 level of $\approx$ 120 ppbv in the outflow region east of the South American continent. Our analysis further shows, that this outflow is associated with strong uplift by convection over South America, mostly over the pristine rain forest of Amazonia. Lightning NO_x emissions certainly contribute to the upper tropospheric O_3 production but they alone are not sufficient to produce the observed mixing ratios. The fractional contribution of biomass burning or LNO_x induced O_3 production is however, difficult to determine. Both source processes underlay a very high variability in space, time and in strength and have generally an uncertainty in their model

https://doi.org/10.5194/egusphere-2025-5372
Preprint. Discussion started: 11 December 2025

representation.

This is in contrast to the assumption by Sauvage et al. (2007) and Jenkins et al. (2021) who assume that lightning produced NO_x dominates O_3 formation in the upper troposphere above 500 hPa causing subsequently the South Atlantic O_3 maximum. Our dataset however, shows not only high O_3 but also very high CO mixing ratios throughout the latitude range between -11° - 30° clearly indicating a contribution of biomass burning to the pollution layer. The layer of enhanced CO mixing ratios can also be seen in the MOPITT satellite dataset in the entire upper troposphere up to 200 hPa. Our findings regarding the O_3 formation processes is in agreement with the study by (Bozem et al., 2017) who conclude that due to convective uplift of precursor gases such as HCHO and H_2O_2, HO_2 mixing ratios can be enhanced in the upper troposphere facilitating O_3 formation. They are also in agreement with an early study of Pickering et al. (1996) who link enhanced O_3 level observed in O_3 soundings from Natal (north Brazilian coastal site) with biomass burning over central Brazil.

The radiative effect of the enhanced upper tropospheric O_3 layer can be considered as significant and is in the same order of magnitude as the shortwave direct aerosol radiative effect induced by African biomass burning aerosol transported over the South East Atlantic (clear sky effect: -0.09 W m^{-2} yr-1, all sky: 0.04 W) (Jouan and Myhre, 2024).

Code and data availability. MOPITT data were obtained from https://www2.acom.ucar.edu/mopitt. GOES data were obtained from https://www.aev.class.noaa.gov/saa/products/welcome;jsessionid=D4234D06E0DA884E3FF16C88A367D13C. The code from MPTRAC is available from https://github.com/slcs-jsc/mptrac. ECMWF's ERA5 data can be freely accessed from https://www.ecmwf.int/en/forecasts/datasets/reanalysis-datasets/era5 (Hersbach et al., 2020). The Modular Earth Submodel System (MESSy) is being continuously further developed and applied by a consortium of institutions. The usage of MESSy and access to the source code is licensed to all affiliates of institutions who are members of the MESSy Consortium. Institutions can become a member of the MESSy Consortium by signing the MESSy Memorandum of Understanding. More information can be found on the MESSy Consortium website (http://www.messy-interface.org).

Author contributions. PH and LS designed the study. LS performed MPTRAC and CAABA simulations and analysed the data. PH, HB, VB, HCL, PJ and DK performed the measurements and prepared the instrument and observational dataset. HT performed the EMAC simulations.

Competing interests. The authors declare that they have no conflict of interest.

Acknowledgements. This research has been supported by the Deutsche Forschungsgemeinschaft (grant no. HO 4225/15-1). The study is a pre-study related to the PHILEAS mission (Probing high Latitude Export from the Asian summer monsoon, HO 4225/19-1) within the HALO-SPP 1294 and was supported by TRR 301 (TPChange , Project-ID 428312742).

https://doi.org/10.5194/egusphere-2025-5372
Preprint. Discussion started: 11 December 2025

References

Abram, N. J., Henley, B. J., Sen Gupta, A., Lippmann, T. J. R., Clarke, H., Dowdy, A. J., Sharples, J. J., Nolan, R. H., Zhang, T., Wooster, M. J., Wurtzel, J. B., Meissner, K. J., Pitman, A. J., Ukkola, A. M., Murphy, B. P., Tapper, N. J., and Boer, M. M. (2021). Connections of climate change and variability to large and extreme forest fires in southeast australia. *Communications Earth and Environment*, 8(2).

Akagi, S. K., Craven, J. S., Taylor, J. W., McMeeking, G. R., Yokelson, R. J., Burling, I. R., Urbanski, S. P., Wold, C. E., Seinfeld, J. H., Coe, H., Alvarado, M. J., and Weise, D. R. (2012). Evolution of trace gases and particles emitted by a chaparral fire in california. *Atmospheric Chemistry and Physics*, 12(3):1397–1421.

Akagi, S. K., Yokelson, R. J., Wiedinmyer, C., Alvarado, M. J., Reid, J. S., Karl, T., Crounse, J. D., and Wennberg, P. O. (2011). Emission factors for open and domestic biomass burning for use in atmospheric models. *Atmospheric Chemistry and Physics*, 11(9):4039–4072.

Andreae, M. O. (2019). Emission of trace gases and aerosols from biomass burning – an updated assessment. *Atmospheric Chemistry and Physics*, 19(13):8523–8546.

Andreae, M. O. and Merlet, P. (2001). Emission of trace gases and aerosols from biomass burning. *Global Biogeochemical Cycles*, 15(4):955–966.

Bourgeois, I., Peischl, J., Neuman, J., Brown, S., Thompson, C., Aikin, K., Allen, H., Angot, H., Apel, E., Baublitz, C., Brewer, J., Campuzano-Jost, P., Commane, R., Crounse, J., Daube, B., DiGangi, J., Diskin, G., Emmons, L., Fiore, A., and Ryerson, T. (2021). Large contribution of biomass burning emissions to ozone throughout the global remote troposphere. *Proceedings of the National Academy of Sciences*, 118:e2109628118.

Bozem, H., Pozzer, A., Harder, H., Martinez, M., Williams, J., Lelieveld, J., and Fischer, H. (2017). The influence of deep convection on hcho and h_2o_2 in the upper troposphere over europe. *Atmospheric Chemistry and Physics*, 17(19):11835–11848.

Cabrera-Perez, D., Taraborrelli, D., Sander, R., and Pozzer, A. (2016). Global atmospheric budget of simple monocyclic aromatic compounds. *Atmospheric Chemistry and Physics*, 16(11):6931–6947.

Chatfield, R. B. and Delany, A. C. (1990). Convection links biomass burning to increased tropical ozone: However, models will tend to overpredict o3. *Journal of Geophysical Research: Atmospheres*, 95(D11):18473–18488.

Crutzen, P. J. (1974). Photochemical reactions initiated by and influencing ozone in unpolluted tropospheric air. *Tellus*, 26(1-2):47–57.

Cuchiara, G., Fried, A., Barth, M., Bela, M., Homeyer, C., Gaubert, B., Walega, J., Weibring, P., Richter, D., Wennberg, P., Crounse, J., Kim, M., Diskin, G., Hanisco, T., Wolfe, G., Beyersdorf, A., Peischl, J., Pollack, I., Clair, J., and Heath, N. (2020). Vertical transport, entrainment, and scavenging processes affecting trace gases in a modeled and observed seac 4 rs case study. *Journal of Geophysical Research: Atmospheres*, 125.

de Oliveira Vieira, S., Satyamurty, P., and Andreoli, R. V. (2013). On the south atlantic convergence zone affecting southern amazonia in austral summer. *Atmospheric Science Letters*, 14(1):1–6.

Deeter, M., Edwards, D., Gille, J., Mao, D., Martínez-Alonso, S., Worden, H., Ziskin, D., and Andreae, M. (2019). Radiance-based retrieval bias mitigation for the mopitt instrument: the version 8 product. *Atmospheric Measurement Techniques*, 12:4561–4580.

Duncan, B. N., Strahan, S. E., Yoshida, Y., Steenrod, S. D., and Livesey, N. (2007). Model study of the cross-tropopause transport of biomass burning pollution. *Atmospheric Chemistry and Physics*, 7(14):3713–3736.

Edwards, D. P., Lamarque, J.-F., Attié, J.-L., Emmons, L. K., Richter, A., Cammas, J.-P., Gille, J. C., Francis, G. L., Deeter, M. N., Warner, J., Ziskin, D. C., Lyjak, L. V., Drummond, J. R., and Burrows, J. P. (2003). Tropospheric ozone over the tropical atlantic: A satellite perspective. *Journal of Geophysical Research: Atmospheres*, 108(D8).

https://doi.org/10.5194/egusphere-2025-5372
Preprint. Discussion started: 11 December 2025

Fiddler, M. N., Thompson, C., Pokhrel, R. P., Majluf, F., Canagaratna, M., Fortner, E. C., Daube, C., Roscioli, J. R., Yacovitch, T. I., Herndon, S. C., and Bililign, S. (2024). Emission factors from wildfires in the western us: An investigation of burning state, ground versus air, and diurnal dependencies during the firex-aq 2019 campaign. *Journal of Geophysical Research: Atmospheres*, 129(1):e2022JD038460. e2022JD038460 2022JD038460.

Fishman, J., Watson, C. E., Larsen, J. C., and Logan, J. A. (1990). Distribution of tropospheric ozone determined from satellite data. *Journal of Geophysical Research: Atmospheres*, 95(D4):3599–3617.

Forster, P. M. d. F. and Shine, K. P. (2002). Assessing the climate impact of trends in stratospheric water vapor. *Geophysical Research Letters*, 29(6):10–1–10–4.

Gilman, J. B., Lerner, B. M., Kuster, W. C., Goldan, P. D., Warneke, C., Veres, P. R., Roberts, J. M., de Gouw, J. A., Burling, I. R., and Yokelson, R. J. (2015). Biomass burning emissions and potential air quality impacts of volatile organic compounds and other trace gases from fuels common in the us. *Atmospheric Chemistry and Physics*, 15(24):13915–13938.

GOES-R Algorithm Working Group and GOES-R Series Program (2018). *NOAA GOES-R Series Geostationary Lightning Mapper (GLM) Level 2 Lightning Detection: Events, Groups, and Flashes. NOAA National Centers for Environmental Information. doi:10.7289/V5KH0KK6*.

GOES-R Series Program (2019). *NOAA GOES-R Series Advanced Baseline Imager (ABI) Level 0 Data. NOAA National Centers for Environmental Information. doi:10.25921/tvws-w071*.

Hersbach, H., Bell, B., Berrisford, P., Hirahara, S., Horányi, A., Muñoz-Sabater, J., Nicolas, J., Peubey, C., Radu, R., Schepers, D., Simmons, A., Soci, C., Abdalla, S., Abellan, X., Balsamo, G., Bechtold, P., Biavati, G., Bidlot, J., Bonavita, M., De Chiara, G., Dahlgren, P., Dee, D., Diamantakis, M., Dragani, R., Flemming, J., Forbes, R., Fuentes, M., Geer, A., Haimberger, L., Healy, S., Hogan, R. J., Hólm, E., Janisková, M., Keeley, S., Laloyaux, P., Lopez, P., Lupu, C., Radnoti, G., de Rosnay, P., Rozum, I., Vamborg, F., Villaume, S., and Thépaut, J.-N. (2020). The era5 global reanalysis. *Quarterly Journal of the Royal Meteorological Society*, 146(730):1999–2049.

Hoffmann, L., Baumeister, P. F., Cai, Z., Clemens, J., Griessbach, S., Günther, G., Heng, Y., Liu, M., Haghighi Mood, K., Stein, O., Thomas, N., Vogel, B., Wu, X., and Zou, L. (2022). Massive-parallel trajectory calculations version 2.2 (mptrac-2.2): Lagrangian transport simulations on graphics processing units (gpus). *Geoscientific Model Development*, 15(7):2731–2762.

Hoffmann, L., Rößler, T., Griessbach, S., Heng, Y., and Stein, O. (2016). Lagrangian transport simulations of volcanic sulfur dioxide emissions: Impact of meteorological data products. *Journal of Geophysical Research: Atmospheres*, 121(9):4651–4673.

Jacob, D. and Winner, D. (2009). Effect of climate change on air quality. *Atmos. Environ.*, 43.

Jaffe, D. A. and Wigder, N. L. (2012). Ozone production from wildfires: A critical review. *Atmospheric Environment*, 51:1–10.

Jenkins, G. S., de Castro, V., Cunha, B., Fontanez, I., and Holzworth, R. (2021). The evolution of the wave-one ozone maximum during the 2017 lasic field campaign at ascension island. *Journal of Geophysical Research: Atmospheres*, 126(10):e2020JD033972. e2020JD033972 2020JD033972.

Jenkins, G. S., Mohr, K., Morris, V. R., and Arino, O. (1997). The role of convective processes over the zaire-congo basin to the southern hemispheric ozone maximum. *Journal of Geophysical Research: Atmospheres*, 102(D15):18963–18980.

Jenkins, G. S. and Ryu, J.-H. (2004). Space-borne observations link the tropical atlantic ozone maximum and paradox to lightning. *Atmospheric Chemistry and Physics*, 4(2):361–375.

Jöckel, P., Tost, H., Pozzer, A., Kunze, M., Kirner, O., Brenninkmeijer, C. A. M., Brinkop, S., Cai, D. S., Dyroff, C., Eckstein, J., Frank, F., Garny, H., Gottschaldt, K.-D., Graf, P., Grewe, V., Kerkweg, A., Kern, B., Matthes, S., Mertens, M., Meul, S., Neumaier, M., Nützel, M.,

https://doi.org/10.5194/egusphere-2025-5372
Preprint. Discussion started: 11 December 2025

Oberländer-Hayn, S., Ruhnke, R., Runde, T., Sander, R., Scharffe, D., and Zahn, A. (2016). Earth system chemistry integrated modelling (escimo) with the modular earth submodel system (messy) version 2.51. *Geoscientific Model Development*, 9(3):1153–1200.

Johansson, S., Wetzel, G., Friedl-Vallon, F., Glatthor, N., Höpfner, M., Kleinert, A., Neubert, T., Sinnhuber, B.-M., and Ungermann, J. (2022). Biomass burning pollution in the south atlantic upper troposphere: Gloria trace gas observations and evaluation of the cams model. *Atmospheric Chemistry and Physics*, 22(5):3675–3691.

Jouan, C. and Myhre, G. (2024). Satellite-based analysis of top of atmosphere shortwave radiative forcing trend induced by biomass burning aerosols over south-eastern atlantic. *npj Clim Atmos Sci*, 7(129).

Kaiser, J. W., Heil, A., Andreae, M. O., Benedetti, A., Chubarova, N., Jones, L., Morcrette, J.-J., Razinger, M., Schultz, M. G., Suttie, M., and van der Werf, G. R. (2012). Biomass burning emissions estimated with a global fire assimilation system based on observed fire radiative power. *Biogeosciences*, 9(1):527–554.

Kirchhoff, V. and Marinho, E. (1994). Layer enhancements of tropospheric ozone in regions of biomass burning. *Atmospheric Environment*, 28(1):69–74.

Kluge, F., Hüneke, T., Knecht, M., Lichtenstern, M., Rotermund, M., Schlager, H., Schreiner, B., and Pfeilsticker, K. (2020). Profiling of formaldehyde, glyoxal, methylglyoxal, and co over the amazon: normalized excess mixing ratios and related emission factors in biomass burning plumes. *Atmospheric Chemistry and Physics*, 20(20):12363–12389.

Koss, A. R., Sekimoto, K., Gilman, J. B., Selimovic, V., Coggon, M. M., Zarzana, K. J., Yuan, B., Lerner, B. M., Brown, S. S., Jimenez, J. L., Krechmer, J., Roberts, J. M., Warneke, C., Yokelson, R. J., and de Gouw, J. (2018). Non-methane organic gas emissions from biomass burning: identification, quantification, and emission factors from ptr-tof during the firex 2016 laboratory experiment. *Atmospheric Chemistry and Physics*, 18(5):3299–3319.

Kunkel, D., Hoor, P., Kaluza, T., Ungermann, J., Kluschat, B., Giez, A., Lachnitt, H.-C., Kaufmann, M., and Riese, M. (2019). Evidence of small-scale quasi-isentropic mixing in ridges of extratropical baroclinic waves. *Atmospheric Chemistry and Physics*, 19:12607–12630.

Leighton, P. (1961). *Photochemistry of Air Pollution*, volume 9. Physical Chemistry.

Liao, J., Wolfe, G. M., Hannun, R. A., St. Clair, J. M., Hanisco, T. F., Gilman, J. B., Lamplugh, A., Selimovic, V., Diskin, G. S., Nowak, J. B., Halliday, H. S., DiGangi, J. P., Hall, S. R., Ullmann, K., Holmes, C. D., Fite, C. H., Agastra, A., Ryerson, T. B., Peischl, J., Bourgeois, I., Warneke, C., Coggon, M. M., Gkatzelis, G. I., Sekimoto, K., Fried, A., Richter, D., Weibring, P., Apel, E. C., Hornbrook, R. S., Brown, S. S., Womack, C. C., Robinson, M. A., Washenfelder, R. A., Veres, P. R., and Neuman, J. A. (2021). Formaldehyde evolution in us wildfire plumes during the fire influence on regional to global environments and air quality experiment (firex-aq). *Atmospheric Chemistry and Physics*, 21(24):18319–18331.

Liebmann, B., Kiladis, G. N., Vera, C. S., Saulo, A. C., and Carvalho, L. M. V. (2004). Subseasonal variations of rainfall in south america in the vicinity of the low-level jet east of the andes and comparison to those in the south atlantic convergence zone. *Journal of Climate*, 17(19):3829 – 3842.

Liu, J., Rodriguez, J. M., Steenrod, S. D., Douglass, A. R., Logan, J. A., Olsen, M. A., Wargan, K., and Ziemke, J. R. (2017). Causes of interannual variability over the southern hemispheric tropospheric ozone maximum. *Atmospheric Chemistry and Physics*, 17(5):3279–3299.

Mauzerall, D. L., Logan, J. A., Jacob, D. J., Anderson, B. E., Blake, D. R., Bradshaw, J. D., Heikes, B., Sachse, G. W., Singh, H., and Talbot, B. (1998). Photochemistry in biomass burning plumes and implications for tropospheric ozone over the tropical south atlantic. *Journal of Geophysical Research: Atmospheres*, 103(D7):8401–8423.

https://doi.org/10.5194/egusphere-2025-5372
Preprint. Discussion started: 11 December 2025

McManus, J. B., Nelson, D. D., Shorter, J. H., Jimenez, R., Herndon, S., Saleska, S., and Zahniser, M. (2005). A high precision pulsed quantum cascade laser spectrometer for measurements of stable isotopes of carbon dioxide. *Journal of Modern Optics*, 52(16):2309–2321.

Moxim, W. J. and Levy II, H. (2000). A model analysis of the tropical south atlantic ocean tropospheric ozone maximum: The interaction of transport and chemistry. *Journal of Geophysical Research: Atmospheres*, 105(D13):17393–17415.

Müller, S., Hoor, P., Berkes, F., Bozem, H., Klingebiel, M., Reutter, P., Smit, H. G. J., Wendisch, M., Spichtinger, P., and Borrmann, S. (2015). In situ detection of stratosphere-troposphere exchange of cirrus particles in the midlatitudes. *Geophysical Research Letters*, 42(3):949–955.

Murray, L. T., Logan, J. A., and Jacob, D. J. (2013). Interannual variability in tropical tropospheric ozone and oh: The role of lightning. *Journal of Geophysical Research: Atmospheres*, 118(19):11,468–11,480.

Nussbaumer, C. M., Crowley, J. N., Schuladen, J., Williams, J., Hafermann, S., Reiffs, A., Axinte, R., Harder, H., Ernest, C., Novelli, A., Sala, K., Martinez, M., Mallik, C., Tomsche, L., Plass-Dülmer, C., Bohn, B., Lelieveld, J., and Fischer, H. (2021). Measurement report: Photochemical production and loss rates of formaldehyde and ozone across europe. *Atmospheric Chemistry and Physics*, 21(24):18413–18432.

Nussbaumer, C. M., Fischer, H., Lelieveld, J., and Pozzer, A. (2023). What controls ozone sensitivity in the upper tropical troposphere? *Atmospheric Chemistry and Physics*, 23(19):12651–12669.

Nussbaumer, C. M., Pozzer, A., Tadic, I., Röder, L., Obersteiner, F., Harder, H., Lelieveld, J., and Fischer, H. (2022). Tropospheric ozone production and chemical regime analysis during the covid-19 lockdown over europe. *Atmospheric Chemistry and Physics*, 22(9):6151–6165.

Parrington, M., Palmer, P. I., Lewis, A. C., Lee, J. D., Rickard, A. R., Di Carlo, P., Taylor, J. W., Hopkins, J. R., Punjabi, S., Oram, D. E., Forster, G., Aruffo, E., Moller, S. J., Bauguitte, S. J.-B., Allan, J. D., Coe, H., and Leigh, R. J. (2013). Ozone photochemistry in boreal biomass burning plumes. *Atmospheric Chemistry and Physics*, 13(15):7321–7341.

Pickering, K., Thompson, A., Wang, Y., Tao, W.-K., McNamara, D., Kirchoff, V., Heikes, B., Sachse, G., Bradshaw, J., Gregory, G., and Blake, D. (1996). Convective transport of biomass burning emissions over brazil during trace-a. *J.Geophys.Res.*, 101:23,993–24,012.

Pickering, K. E., Wang, Y., Tao, W.-K., Price, C., and Müller, J.-F. (1998). Vertical distributions of lightning nox for use in regional and global chemical transport models. *Journal of Geophysical Research: Atmospheres*, 103(D23):31203–31216.

Pickering, K.E., T.-A. S. J. a. W.-K. T. and Simpson, J. (1992). Ozone production potential following convective redistribution of biomass burning emissions. *Journal of Atmospheric Chemistry*, 14:297–313.

Pozzer, A., Jöckel, P., and Van Aardenne, J. (2009). The influence of the vertical distribution of emissions on tropospheric chemistry. *Atmospheric Chemistry and Physics*, 9(24):9417–9432.

Pöschl, U., Kuhlmann, R., Poisson, N., and Crutzen, P. (2000). Development and intercomparison of condensed isoprene oxidation mechanisms for global atmospheric modeling. *Journal of Atmospheric Chemistry*, 37:29–52.

Rap, A., Richards, N. A. D., Forster, P. M., Monks, S. A., Arnold, S. R., and Chipperfield, M. P. (2015). Satellite constraint on the tropospheric ozone radiative effect. *Geophysical Research Letters*, 42(12):5074–5081.

Rapp, M., Kaifler, B., Dörnbrack, A., Gisinger, S., Mixa, T., Reichert, R., Kaifler, N., Knobloch, S., Eckert, R., Wildmann, N., Giez, A., Krasauskas, L., Preusse, P., Geldenhuys, M., Riese, M., Woiwode, W., Friedl-Vallon, F., Sinnhuber, B.-M., de la Torre, A., Alexander, P., Hormaechea, J. L., Janches, D., Garhammer, M., Chau, J. L., Conte, J. F., Hoor, P., and Engel, A. (2021). Southtrac-gw: Gravity waves meet sudden stratospheric warming. *Bulletin of the American Meteorological Society*, 102(12):1158 – 1166.

https://doi.org/10.5194/egusphere-2025-5372
Preprint. Discussion started: 11 December 2025

Real, E., Law, K. S., Weinzierl, B., Fiebig, M., Petzold, A., Wild, O., Methven, J., Arnold, S., Stohl, A., Huntrieser, H., Roiger, A., Schlager, H., Stewart, D., Avery, M., Sachse, G., Browell, E., Ferrare, R., and Blake, D. (2007). Processes influencing ozone levels in alaskan forest fire plumes during long-range transport over the north atlantic. *Journal of Geophysical Research: Atmospheres*, 112(D10).

Riede, H., Jöckel, P., and Sander, R. (2009). Quantifying atmospheric transport, chemistry, and mixing using a new trajectory-box model and a global atmospheric-chemistry gcm. *Geoscientific Model Development*, 2(2):267–280.

Riese, M., Ploeger, F., Rap, A., Vogel, B., Konopka, P., Dameris, M., and Forster, P. (2012). Impact of uncertainties in atmospheric mixing on simulated utls composition and related radiative effects. *Journal of Geophysical Research*, 117.

Sander, R., Baumgaertner, A., Cabrera-Perez, D., Frank, F., Gromov, S., Grooß, J.-U., Harder, H., Huijnen, V., Jöckel, P., Karydis, V. A., Niemeyer, K. E., Pozzer, A., Riede, H., Schultz, M. G., Taraborrelli, D., and Tauer, S. (2019). The community atmospheric chemistry box model caaba/mecca-4.0. *Geoscientific Model Development*, 12(4):1365–1385.

Sauvage, B., Martin, R. V., van Donkelaar, A., Liu, X., Chance, K., Jaeglé, L., Palmer, P. I., Wu, S., and Fu, T.-M. (2007). Remote sensed and in situ constraints on processes affecting tropical tropospheric ozone. *Atmospheric Chemistry and Physics*, 7(3):815–838.

Sauvage, B., Thouret, V., Thompson, A. M., Witte, J. C., Cammas, J.-P., Nédélec, P., and Athier, G. (2006). Enhanced view of the "tropical atlantic ozone paradox" and "zonal wave one" from the in situ mozaic and shadoz data. *Journal of Geophysical Research: Atmospheres*, 111(D1).

Schill, G., Froyd, K., Bian, H., Kupc, A., Williamson, C., Brock, C., Ray, E., Hornbrook, R., Hills, A., Apel, E., Chin, M., Colarco, P., and Murphy, D. (2020). Widespread biomass burning smoke throughout the remote troposphere. *Nature Geoscience*, 13.

Schumann, U. and Huntrieser, H. (2007). The global lightning-induced nitrogen oxides source. *Atmospheric Chemistry and Physics*, 7(14):3823–3907.

Seinfeld, J. and Pandis, S. (2016). *Atmospheric Chemistry and Physics: From Air Pollution to Climate Change*. Wiley.

Sillman, S. (1995). The use of no , h2o2, and hno3 as indicators for ozone-no -hydrocarbon sensitivity in urban locations. *Journal of Geophysical Research: Atmospheres*, 100(D7):14175–14188.

Sillman, S. (1999). The relation between ozone, nox and hydrocarbons in urban and polluted rural environments. *Atmospheric Environment*, 33(12):1821–1845.

Tadic, I., Crowley, J. N., Dienhart, D., Eger, P., Harder, H., Hottmann, B., Martinez, M., Parchatka, U., Paris, J.-D., Pozzer, A., Rohloff, R., Schuladen, J., Shenolikar, J., Tauer, S., Lelieveld, J., and Fischer, H. (2020). Net ozone production and its relationship to nitrogen oxides and volatile organic compounds in the marine boundary layer around the arabian peninsula. *Atmospheric Chemistry and Physics*, 20(11):6769–6787.

Thompson, A. M., Witte, J. C., Sterling, C., Jordan, A., Johnson, B. J., Oltmans, S. J., Fujiwara, M., Vömel, H., Allaart, M., Piters, A., Coetzee, Gert J. R. a nd Posny, F., Corrales, E., Diaz, J. A., Félix, C., Komala, N., Lai, Nga a nd Ahn Nguyen, H. T., Maata, M., Mani, F., Zainal, Z., Ogino, S.-y., Paredes, F., Penha, T. L. B., da Silva, F. R., Sallons-Mitro, S., Selkirk, H. B., Schmidlin, F. J., Stübi, R., and Thiongo, K. (2017). First reprocessing of southern hemisphere additional ozonesondes (shadoz) ozone profiles (1998–2016): 2. compa risons with satellites and ground-based instruments. *Journal of Geophysical Research: Atmospheres*, 122(23):13,000–13,025.

Tonnesen, G. S. and Dennis, R. L. (2000). Analysis of radical propagation efficiency to assess ozone sensitivity to hydrocarbons and no : 2. long-lived species as indicators of ozone concentration sensitivity. *Journal of Geophysical Research: Atmospheres*, 105(D7):9227–9241.

Torres, O., Chen, Z., Jethva, H., Ahn, C., Freitas, S. R., and Bhartia, P. K. (2010). Omi and modis observations of the anomalous 2008–2009 southern hemisphere biomass burning seasons. *Atmospheric Chemistry and Physics*, 10(8):3505–3513.

Ulke, A., Longo de Freitas, K., and Freitas, S. (2011). *Biomass Burning in South America: Transport Patterns and Impacts*, volume 19.

https://doi.org/10.5194/egusphere-2025-5372
Preprint. Discussion started: 11 December 2025

van Vuuren, D., Edmonds, J., Kainuma, M., Riahi, K., Thomson, A., Hibbard, K., Hurtt, G., Kram, T., Krey, V., Lamarque, J.-F., Masui, T., Meinshausen, M., Nakicenovic, N., Smith, S., and Rose, S. (2011). The representative concentration pathways: an overview. climatic change. this issue. *Climatic Change*, 109:5–31.

Vera, C., Higgins, W., Amador, J., Ambrizzi, T., Garreaud, R., Gochis, D., Gutzler, D., Lettenmaier, D., Marengo, J., Mechoso, C. R., Nogues-Paegle, J., Dias, P. L. S., and Zhang, C. (2006). Toward a unified view of the american monsoon systems. *Journal of Climate*, 19(20):4977 – 5000.

Villela, R. (2017). The south atlantic convergence zone: a critical view and overview. *Revista do Instituto Geológico*, 38.

Watson, C. E., Fishman, J., and Reichle Jr., H. G. (1990). The significance of biomass burning as a source of carbon monoxide and ozone in the southern hemisphere tropics: A satellite analysis. *Journal of Geophysical Research: Atmospheres*, 95(D10):16443–16450.

Wentworth, G. R., abeba Aklilu, Y., Landis, M. S., and Hsu, Y.-M. (2018). Impacts of a large boreal wildfire on ground level atmospheric concentrations of pahs, vocs and ozone. *Atmospheric Environment*, 178:19–30.

Witte, J. C., Thompson, A. M., Smit, H. G. J., Fujiwara, M., Posny, F., Coetzee, G. J. R., Northam, E. T., Johnson, B. J., Sterling, C. W., Mohamad, M., Ogino, S.-Y., Jordan, A., and da Silva, F. R. (2017). First reprocessing of southern hemisphere additional ozonesondes (shadoz) profile records (1998–2015): 1. methodology and evaluation. *Journal of Geophysical Research: Atmospheres*, 122(12):6611–6636.

Xia, Y., Huang, Y., and Hu, Y. (2018). On the climate impacts of upper tropospheric and lower stratospheric ozone. *Journal of Geophysical Research: Atmospheres*, 123(2):730–739.

Yue, X., Mickley, L. J., Logan, J. A., Hudman, R. C., Martin, M. V., and Yantosca, R. M. (2015). Impact of 2050 climate change on north american wildfire: consequences for ozone air quality. *Atmospheric Chemistry and Physics*, 15(17):10033–10055.

Zahn, A., Weppner, J., Widmann, H., Schlote-Holubek, K., Burger, B., Kühner, T., and Franke, H. (2012). A fast and precise chemiluminescence ozone detector for eddy flux and airborne application. *Atmospheric Measurement Techniques*, 5(2):363–375.

Ziereis, H., Hoor, P., Grooß, J.-U., Zahn, A., Stratmann, G., Stock, P., Lichtenstern, M., Krause, J., Bense, V., Afchine, A., Rolf, C., Woiwode, W., Braun, M., Ungermann, J., Marsing, A., Voigt, C., Engel, A., Sinnhuber, B.-M., and Oelhaf, H. (2022). Redistribution of total reactive nitrogen in the lowermost arctic stratosphere during the cold winter 2015/2016. *Atmospheric Chemistry and Physics*, 22(5):3631–3654.